INTERNATIONAL JOURNAL OF SOCIAL SCIENCE EXCEPTIONAL RESEARCH

Research on the effect of control angle on aerodynamic forces applied to cars using the Les Method and CFD application simulation

Nguyen Tri Nguyen [1], Le Thi Minh Nghia [2], Bui Quoc Khoa [3*], Nguyen Chi Cong [4], Pham Minh Vuong [5], Le Thi Minh Nghia [6]

[1] Nong Lam University, HCMC, Vietnam

[2] Institute for Computational Science and Technology, Vietnam

[3] Van Lang University, Vietnam

[4, 5, 6] Ho Chi Minh City University of Technology, Vietnam

* Corresponding Author: **Bui Quoc Khoa**

Article Info

ISSN (online): 2583-8261
Volume: 04
Issue: 01
January-February 2025
Received: 09-11-2024
Accepted: 10-12-2024
Page No: 36-46

Abstract

In this paper, the Large Eddy Simulation (LES) flow modeling technique is used to solve the Navier-Stokes equations. In this, the effect of the stress components from the small structures is modeled by the Smagorinsky flow model. This mathematical model is used for the flow through a square cylinder at two different Reynolds number conditions Re = 400 and Re = 22,000. The computed results of the average flow and the features of the multi-dynamic components are compared with the results obtained from the DNS (Direct Numerical Simulation) method and the k-ε model, demonstrating the benefits of this method. Simultaneously, these results also align well with the experimental results at the same Reynolds number conditions.

Nowadays, the automobile industry is increasingly developing, along with the requirements of reducing fuel consumption, the design of cars with good aerodynamic shape is of interest to many countries in the world. Therefore, reducing aerodynamic drag is one of the issues that car designers put first. The method of simulating fluid flow through the car uses the finite volume method for unstructured mesh, using Fluent software based on the Reynolds Navier - Stokes average equation and the standard k - ε turbulence model. The accuracy of the problem depends on the number of grid points and the computer resources. The problem is solved by the sequential solution method. The simulation results are shown in intuitive graphics, which are the pressure and velocity distribution fields.

DOI: https://doi.org/10.54660/IJSSER.2025.4.1.36-46

Keywords: CFD simulation, Computational Fluid Dynamic, Turbulent air flow, maneuver angle car, air movement through the car

1. Introduction

For many years, flow modeling techniques using the Reynolds Averaged Navier-Stokes (RANS) equations along with models like k-ε or Q-ω have been the only options to simulate and calculate flow in industrial settings. The benefit of using models based on the Reynolds Navier-Stokes average equations is that they involve relatively low computational effort and can be utilized with existing computing tools to obtain average flow characteristics. The drawback of these models is that the calculation's time response does not align with the actual flow's time response. Additionally, for these models, five to seven numerical terms are needed in the Reynolds-averaged equation, which depends on factors such as flow type, Reynolds number, and fluid type, each requiring different numerical terms.

Recently, the model-free Direct Numerical Simulation (DNS) approach to solving the Navier-Stokes equations has been examined for many types of flows. The benefit of this approach is that it precisely represents the time changes of the flow and the average values. The downside of the approach is that the computational expense is very high. Piomeli [1] calculated the amount of points needed for a three-dimensional moving flow in space using the DNS method at a scale of Re9/4. With the power of modern computers, this method can only simulate a few simple flows with low Reynolds numbers of several thousand.

To solve the difficulties of the two flow modeling methods mentioned above, currently, the flow modeling method according to large structures (Large Eddy Simulation - LES) is being researched and used in many problems and in the future will be used in many flow calculation software. This LES method is based on the basic principle of directly calculating only large flow structures, while small structures will be modeled. Therefore, with the LES method, the modeling process only requires a moderate amount of calculation to be able to calculate large structures - structures that characterize the flow motion characteristics.

In this paper, the LES flow model with the Smagorinsky flow model [2] is applied to solve the problem over a square. The computational results will be compared with the experimental results by Lyn *et al*. [3, 4] and Durao *et al*. [5], showing the good agreement of the model with the experimental results. This is the first part of the research on the LES method and is only applied to the flow through a simple square body, but it is also the foundation for the next research parts of this method for complex bodies applied in the industrial field later (flow through hydraulic machines, turbines, aircraft blades, etc.)

Nowadays, with the strong development of the automobile industry, the number of cars in circulation in the world is increasing, so the use of fuel in the world is increasing, making the amount of oil in nature increasingly depleted. Therefore, this is also a problem for car designers, producing cars with the most economical fuel consumption. (Lamballais E., Sylvestrini S.H., 2002) [1].

There are many measures to reduce fuel consumption in cars such as designing engines with low fuel consumption, engines using different energy sources and designing cars with suitable shapes to have the smallest drag coefficient (Cd). (Pham M.V., Plourde F. and Doan Kim S., 2003) [2].

Using numerical methods in finding solutions for engineering problems has been used more widely and more accurately. Among those methods, the most prominent are methods such as: Finite Element Method, Finite Difference Method, and Boundary Element Method. Especially for problems related to hydrodynamics, people use the Finite Volume Method.

In this paper, we introduce some results of calculating the change in the drag coefficient in the case of changing the car's maneuvering angle using FLUENT software. These results will be used to evaluate the established integral model.

2. Theoretical basis

2.1. LES method Theoretical

2.1.1. LES Turbulent flow simulation

In the LES shear modelling method, shear structures with larger excitations than the shear size are modelled directly, while those with smaller excitations than the shear size are modelled. To distinguish between large and small shear structures and to model the influence of small shear structures on large shear structures, a force function is applied to the Navier-Stokes equations. With this function, a physical quantity f in the equation will be divided into two parts; one filtered part $\overline{f}$, which represents the large-scale structure, will be calculated directly from the equation f', the other part, which represents the small-scale structure, will be modeled: $f = \overline{f} + f'$.

In which, the large-scale structure component $\overline{f}$ has been filtered when applying a filter function as follows:

$$\overline{f}(\mathbf{x}) = \frac{1}{\prod_{i=1}^{3}\Delta_i(\mathbf{x})}\int_{\Omega}\prod_{i=1}^{3}G_i\left(\frac{x_i - y_i}{\Delta_i(\mathbf{x})}, \mathbf{x}\right)f(\mathbf{y})d^3\mathbf{y} \qquad (1.1)$$

Apply this equation to the continuity equation and the momentum equation:

$$\frac{\partial \overline{u}_i}{\partial x_i} = 0 \qquad (1.2)$$

$$\frac{\partial \overline{u}_i}{\partial t} + \frac{\partial \overline{(u_i u_j)}}{\partial x_j} = -\frac{1}{\rho}\frac{\partial \overline{p}}{\partial x_i} + \frac{\partial}{\partial x_j}\left[\nu\left(\frac{\partial \overline{u}_i}{\partial x_j} + \frac{\partial \overline{u}_j}{\partial x_i}\right)\right] \qquad (1.3)$$

The momentum equation after being applied will give rise to a quantity that models the nonlinear interaction of two velocity components in the directions i and j: $\overline{u_i u_j}$.

One of the advantages of the LES method is that the kinetic equation after being translated can be written as the equation of motion of large-scale elements.

$$\frac{\partial \overline{u}_i}{\partial t} + \frac{\partial \overline{u}_i\overline{u}_j}{\partial x_j} = -\frac{1}{\rho}\frac{\partial \overline{p}}{\partial x_i} + \nu\frac{\partial^2 \overline{u}_i}{\partial x_j \partial x_j} - \frac{\partial \tau_{ij}}{\partial x_j} \qquad (1.4)$$

In which: $\tau_{ij} = \overline{u_i u_j} - \overline{u}_i\overline{u}_j$, called the «substructure tensor», the influence of the velocity components of the small structure, which are not directly solved, on the velocity components of the large structure is modeled. This unknown quantity will be modeled.

In practice, the tensor under stress can be decomposed into its deviatoric stress components $\tau_{ij}^D = \tau_{ij} - 1/3\,\tau_{kk}\delta_{ij}$ and the effects of the main component on the pressure quantity $\overline{p}^* = \overline{p} + 1/3\,\tau_{kk}$. The resulting equation is of the form:

$$\frac{\partial \overline{u}_i}{\partial t} + \frac{\partial \overline{u}_i\overline{u}_j}{\partial x_j} = -\frac{1}{\rho}\frac{\partial \overline{p}^*}{\partial x_i} + \nu\frac{\partial^2 \overline{u}_i}{\partial x_j \partial x_j} - \frac{\partial \tau_{ij}^D}{\partial x_j} \qquad (1.5)$$

The system of equations and will be closed when the shear stress component is modeled by the shear stress model according to Boussinesq's hypothesis:

$$-\nabla.\tau^D = \nabla.\left(\nu_T\left(\nabla\overline{u} + \nabla^T\overline{u}\right)\right) \qquad (1.6)$$

or: $\tau_{ij}^{D} = -2\nu_T \bar{S}_{ij}$ (1.7)

In which the smallest, ν_T , will be calculated according to the Smagorinsky model [2].

$$\nu_T = \left(C_S \bar{\Delta}\right)^2 \left|\bar{S}\right| = \left(C_S \bar{\Delta}\right)^2 \left(2\bar{S}_{ij}\bar{S}_{ij}\right)^{1/2} \quad (1.8)$$

With C_S which It is called the Smagorinsky number. According to the theory of homogeneous and uniform motion, this number is determined $C_S \cong 0.18$. However, in many recent studies, authors have proposed to use $C_S \cong 0.15$.

The final equation has the form:

$$\frac{\partial \bar{u}_i}{\partial x_i} = 0 \quad (1.9)$$

$$\frac{\partial \bar{u}_i}{\partial t} + \frac{\partial \bar{u}_i \bar{u}_j}{\partial x_j} = -\frac{1}{\rho}\frac{\partial \bar{p}^*}{\partial x_i} + \left(\nu + \nu_T\right)\frac{\partial^2 \bar{u}_i}{\partial x_j \partial x_j} \quad (1.10)$$

Thus the system of equations and will be closed by Smagorinsky's model.

2.1.2. Numerical calculation diagram

The Navier Stokes equations with the LES model are solved in a uniformly distributed computational domain in a Decart system by the finite difference method. The spatial scheme is a second-order exact central difference scheme. The temporal difference scheme is a Mac-Cormack scheme with two-step prediction and correction of second-order accuracy. The continuity and momentum equations are solved by the projection method of Najm *et al.* [6] to derive the Poisson equation. This Poisson equation is solved by the differential equation method to find the pressure, which is then introduced into the momentum and continuity equations to find the velocity components of the flow. The stability condition of the differential equation in this calculation is the condition CFL = 0.3 according to Pham *et al.* [7].

2.1.3. Boundary condition calculation configuration

The computational domain of the simple problem is a rectangular prism of dimensions L_x , L_y , L_z in three directions of velocity u_x , u_y , u_z in three-dimensional space as . The rectangular prism of dimensions D is placed parallel to the axis Z of the rectangular prism. This prism problem is solved in three dimensional computational space with different numbers of solutions depending on the Reynolds number presented above.

Table 1: Calculation, division and timing configuration

Reynolds	D (m)	L_x x L_y x L_z	N_x x N_y x N_z	Δt (s)
400	5.10^{-4}	24D x 8D x 12D	192 x 128 x 96 x $2,4.10^{6}$	10^{-6}
22000	2.10^{-3}	15D x 7D x 1,5D	400 x 256 x 32 x $3,3.10^{6}$	10^{-5}

The input variable condition of the problem is a uniform flow with velocity $\vec{U}_0$. To create conditions for the flow to develop, the input velocity of the problem has a dynamic component of about 0.1%, this condition is also suitable for the conditions in reality as well as in experiments. The boundary conditions on the two sides of the perpendicular region with respect to the direction Y are symmetrical boundary conditions. The boundary conditions on the top and bottom sides of Z the perpendicular region with respect to the direction Z are periodic because in this case we assume an infinitely long cylindrical geometry in the direction and this problem only solves a part of the cylindrical geometry. The output condition of the computational domain is the passive flow condition (whatever the flow inside is, the flow outside will have its properties preserved). And finally the flow condition on the diagram is the zero velocity components.

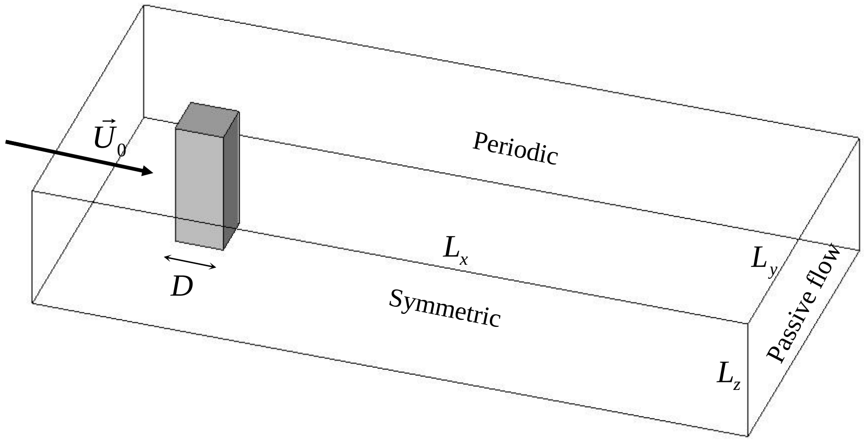

Fig 1: Computational configuration and conditions

2.1.4. Experience of Medium turbulent airflow and LES time Response Capability

2.1.4.1. Medium and turbulent airflow

As introduced in the previous section, in this paper the LES model is used to simulate the flow around a square cylinder in two cases with different Reynolds numbers. The effect of Reynolds number on the flow structure around the square cylinder will be discussed in the final section of the paper. In this section we will only discuss the flow through the diaphragm at Reynolds Re = 22,000 to be able to compare it with the experimental results as well as with other results calculated $k-\varepsilon$ by the Reynolds-averaged model. In this calculation, the flow around the cylinder is modeled in terms of the total time of the flow being 0.4s, of which the first 0.1s is the time required for the flow to reach a steady state from an initial velocity of zero. The remaining time 0.3s is the time that the current has reached a steady state, and the average value is calculated from the average of all the values in the 0.3s steady state of the current.

The mean velocity in the flow direction (direction X) on the symmetric plane of the cylinder is shown in Fig. The results calculated by the LES model are also compared with the experimental results at the same Reynolds number condition Re = 22,000 performed by Lyn *et al.* [3, 4] and Durao *et al.* [5]. This comparison shows that the results calculated by the LES model are in close agreement with the experimental results of Lyn *et al.* [3, 4] in the front part of the figure. The back part of the figure shows a difference of about 5% to 10% between the calculated and experimental results.

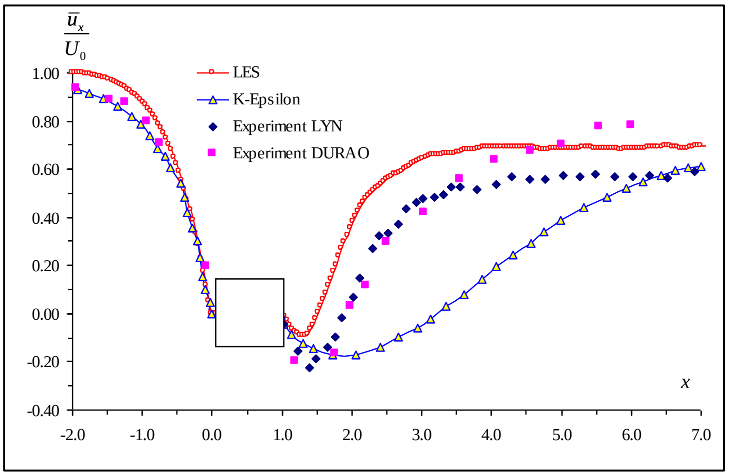

Fig 2: *Distribution in the direction X of mean velocity* $\bar{u}_x$

In this case, if we compare the results calculated by the LES model k-ε applied to the Reynolds Navier Stokes average equation with the experimental results, there is a very large difference of up to 50% in the velocity part behind the image. While the velocity part in front of the image k-ε calculated from the LES model and the experimental results are almost the same. This is also easily explained because the LES model is used to simulate and respond well over time so that it can accommodate the very large velocity variations after the deformation caused by the Von-Karman vortices. While the model k-ε applied to the Reynolds average equation has a poor time response (due to averaging the equation), it can only give good results for the pre-rotation velocity (because there is little noise) and significant errors for the post-rotation velocity, where there is a significant noise component. This will be discussed in more detail in the following section.

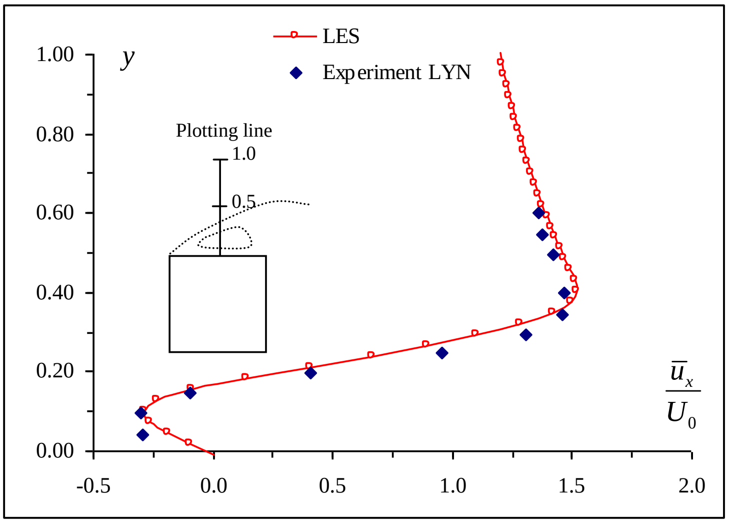

Fig 3: The distribution Y of the mean velocity curve on the upper surface $\bar{u}_x$

Another result in a relatively complex region is also presented, which is a square rotation on both sides, to show the adaptation of the LES model. This rotation lies on a very thin layer on both sides of the square. The LES calculation results are similar to the experimental results obtained by Lyn *et al.* [3, 4] The y-direction average velocity $\overline{u}_x$ profile of Fig. 3 at point $x = 0,5D$ a shows the adaptation of the LES model. Physically, the phenomenon of boundary layer separation of the trough layer near the shear wall creates a reverse flow in this region $u_x < 0$ and the flow returns to normal $u_x < 0$ when $u_x > 0$. With the above comparisons of the average current, the LES method gives results close to the experimental results.

Not only for the average value but also for the currents or for the idle currents the dynamic component plays a very important role. This dynamic component is represented by the dynamic energy of the current: $k = \frac{1}{2}\left(\overline{u_x'^2} + \overline{u_y'^2} + \overline{u_z'^2}\right)$ on the symmetrical plane shown in Figure 4.

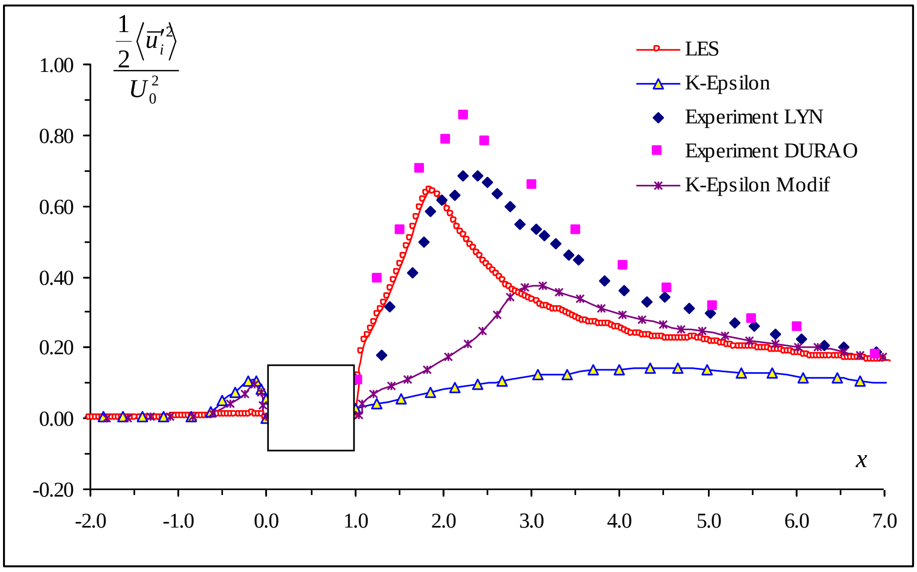

Fig 4: Divide the raft according X to the direction of the gate

The calculated results of the dynamic response using the LES method are consistent with the experimental results by Lyn *et al.* [3, 4] and by Durao *et al.* [5]. Once again the comparison of the model k-ε with the calculated results of the kinetic energy obtained from the multi-velocity components behind the image shows the limitations of the model k-ε with both non-uniform flows and kinetic flows. In this case, the calculated result of the dynamic force by the model k-ε by Franke and Rodi [8] after the regression only achieved the largest value of about 0.1 while the experimental results as well as the results calculated by the LES method were in the range $0,6 \div 0,7$ shown in Figure 4. Even with the corrected model k-ε by Lamder and Kato [9], this value only achieved about 0.4. Thus, in terms of mean and dynamic range, the LES method has a remarkable agreement with the experimental results while the model k-ε has a certain limited capability.

2.1.4.2. LES Time Response Capability

To investigate the variation of quantities with time, as well as with frequency, in this section the method of frequency spectrum analysis of velocity signals is applied to determine the frequency variation of the stream. Figure 5(a) shows the frequency spectrum at point A located at the position $x = 0,5D$ and $y = 0,75D$ within the lateral rotation region of the figure. The energy at this point has a maximum at frequency $f = 115hz$ and has the form of the energy of the free current. The value of this frequency corresponds to the Strouhal number $St = \frac{fD}{U_0} = 0,14$, which is the integer frequency of the Von-Karman vortex after the rotation. Comparison with the experimental results of Lyn *et al.* [3, 4] with $St = 0,132$, Durao *et al.* [5] with $St = 0,139$ shows the compatibility of this calculation result.

The frequency spectrum of a point B located behind the hexagonal prism $X = 11D, y = 0$ is shown in Figure 5(b). At this point, the frequency spectrum has no maximum value as seen in the region near the hexagonal prism, and the slope of the frequency spectrum on the logarithm is -5/3. The slope value of -5/3 indicates a Kolmogorov structure in this directional region. This analysis shows the evolution of the flow from layer to layer, and it also shows the capture of the flow structures of the LES method.

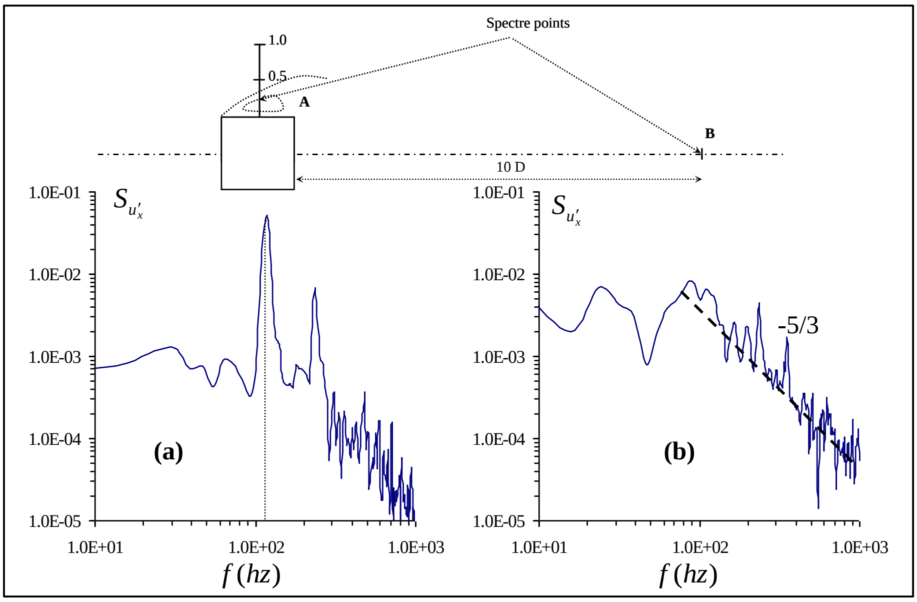

Fig 5: The energy density at two points A and B.

2.1.4.3. Reynolds flow structure

In terms of physics, in order to easily see the development of the flow structure, the calculation method and the representation of the turbulence field $\omega = \sqrt{\omega_x^2 + \omega_y^2 + \omega_z^2}$ are considered in this section. As mentioned in the introduction, the influence of the Reynolds number on the flow structure is also analyzed in this section, namely the two Reynolds numbers $\mathrm{Re} = 22\,000$ and $\mathrm{Re} = 400$. Figure 6(a) shows the isosurface of the vortex field $\omega = 5000\,(s^{-1})$ corresponding to $\mathrm{Re} = 22\,000$. In this case, in the region near the cylinder the flow structure is laminar with large structures. Farther behind the cylinder, these large structures overlap and are collapsed into small, laminar structures.

In contrast, in the case of the small Reynolds number $\mathrm{Re} = 400$ shown in Figure 6(b) $\omega = 30000\,(s^{-1})$, the near-circular flow structures are two-dimensional vortex tubes with longitudinal axis produced by the separation of the boundary layers. These two-dimensional vortex tubes are separated from the circular shape and deform into curved vortex structures in space as they move away from the circular shape. In addition, between these longitudinally curved vortex tubes, there are also vortex fibers entrained in the direction of flow caused by the deformation of the longitudinally curved vortex tubes. It is noteworthy here that, although they are entrained in each other, these vortex structures are not crushed in the case $\mathrm{Re} = 22\,000$; showing the structure of a laminar flow. This structure is also a laminar flow structure obtained from the direct solution of the Navier-Stokes (DNS) equations by Lambalais *et al.* [10] together with Reynolds.

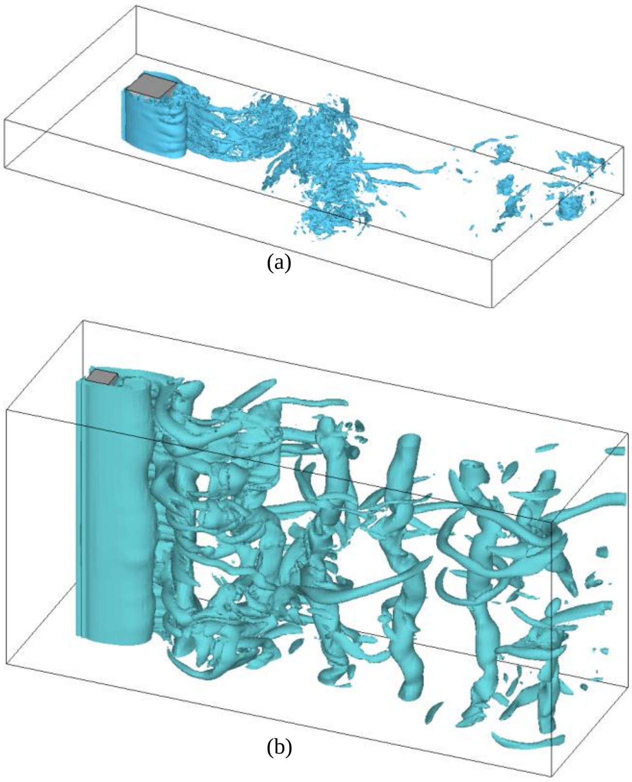

Fig 6: Structure of air flow moving through cylindrical structure

2.2. Simulation method

2.2.1. Turbulence model k – ε

The standard model uses the following two equations for and ε:

$$\frac{\partial(\rho k)}{\partial t} = div(\rho k U) = div\left(\frac{\mu_t}{\sigma_k} gradk\right) + G_k - \rho\varepsilon \qquad (1.11)$$

$$\frac{\partial(\rho\varepsilon)}{\partial t} = div.(\rho\varepsilon U) = div.\left(\frac{\mu_t}{\sigma_\varepsilon} grad.\varepsilon\right) + C_{1\varepsilon}\frac{\varepsilon}{k}G_k - C_{2\varepsilon}\rho\frac{\varepsilon^2}{k} \qquad (1.12)$$

With: G_k is a quantity characterizing the turbulence dynamics (for every type of turbulence model this characteristic will be different), $C_{1\varepsilon}$, $C_{2\varepsilon}$: adjustable constants,: $\sigma_k, \sigma_\varepsilon$ are Prandtl coefficients for k and ε, respectively.

2.2.2. Computational model

The car type selected for the calculation is Mercedes-Benz C180K CLASSIC, with parameters as in Table 1.

Table 2: Mercedes-Benz C180K CLASSIC car parameters

No.	Parameter	Value
01	Length basic (m)	2,715
02	Length (m)	4,652
03	Width (m)	1,728
04	High (m)	1,426
05	Distance from front axle to front of vehicle (m)	0,755
06	Distance from rear axle to rear of vehicle (m)	1,056
07	Wind resistance coefficient C_d	0,26
08	Total weight (kg)	1,965

The car moves on the road, so the car will move through the air stream. The air has a viscosity coefficient μ= $1.789.10^{-5}$ kg/m.s, and a density of ρ = 1.225 kg/m^3. The car moves at a speed of 40 m/s, corresponding to a Reynolds number of 4.10^6. The calculation space has dimensions selected as shown in Figure 1.

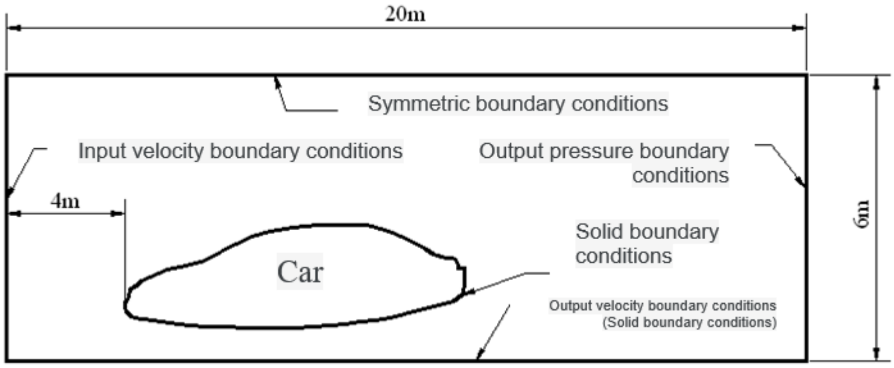

Fig 7: Computational space and boundary conditions

2.2.3. Meshing and boundary conditions

Mesh division: The density of the mesh has a great influence on the calculation results. In the area near the solid wall, the fluid changes greatly, so the mesh density here needs to be divided more finely to clearly show the change of the flow. The finer the mesh, the more clearly it shows the change of the flow and reduces the calculation error.

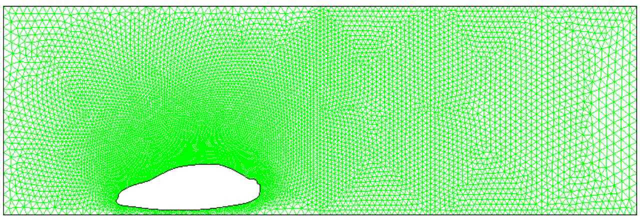

Fig 8: Spatial discrete model computed by Gambit with 17540 points

Boundary conditions: The boundary conditions of the computational domain are determined as shown in Figure 1, the values assigned to these boundary conditions are shown in Tables 2 & 3.

Table 3: Input velocity boundary conditions

Velocity (m/s)	$\vec{r}$	T (K)	I (%)	L (m)
40	(1,0,0)	303	5	0,05

Table 4: Outlet pressure boundary conditions

P (Pa)	T (K)	I (%)	L (m)
$9,81.10^4$	303	5	0,05

In which: I is the turbulence intensity, L is the characteristic turbulence length, temperature and pressure are selected according to actual external conditions.

1. Result

In this section, the author studies how changes in the front maneuver angle and rear maneuver angle affect aerodynamic properties? The choice of the computational space and boundary conditions is the same as above. The author will simulate a car running at a speed of 40 m/s. Consider a car with a front maneuver angle (α) and a rear maneuver angle (β) as shown in Figure 3. (Lamballais E., Sylvestrini S.H., 2002) [10].

Fig 9: Car shape with front and rear maneuverability angles

3.1. Effect of forward maneuver angle (α)

In this section, we consider the effect of aerodynamic forces acting on the car when the front maneuver angle changes, the rear maneuver angle β = 27^0.

The simulation results are as follows

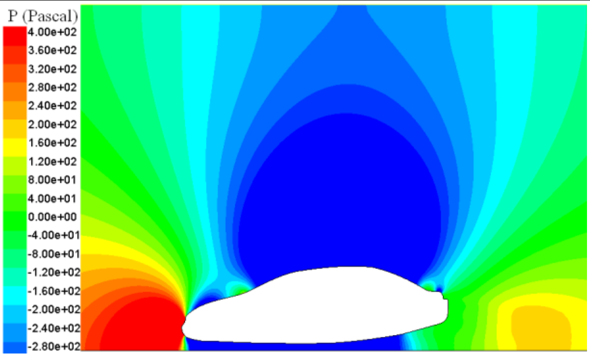

Fig 10: Pressure distribution on the calculation domain when α =18^0

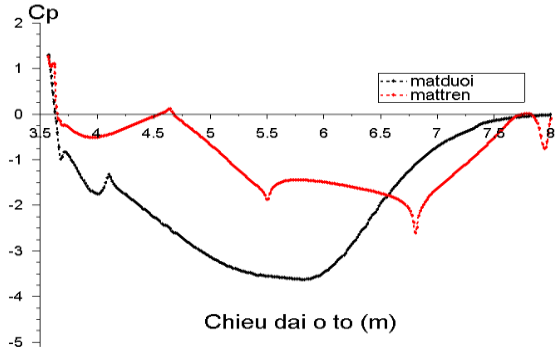

Fig 11: Distribution of pressure distribution coefficient on car when α =18^0

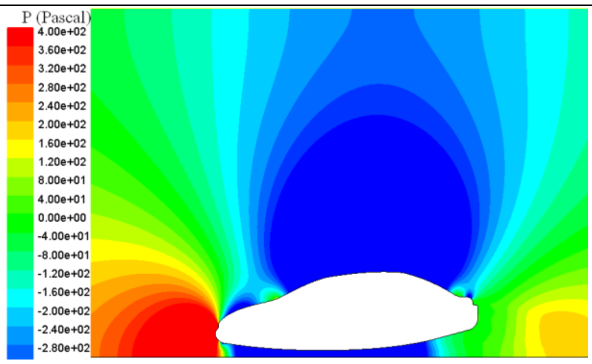

Fig 12: Pressure distribution on the calculation domain when α =20^0

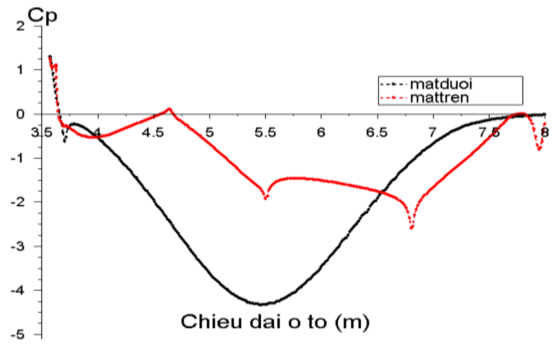

Fig 13: Pressure coefficient distribution on car when α =20^0

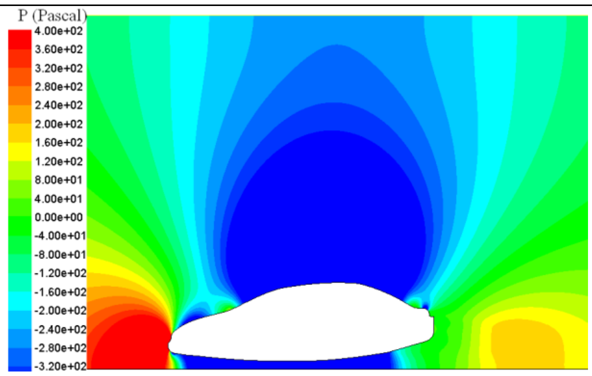

Fig 14: Pressure distribution on the calculation domain when α =22^0

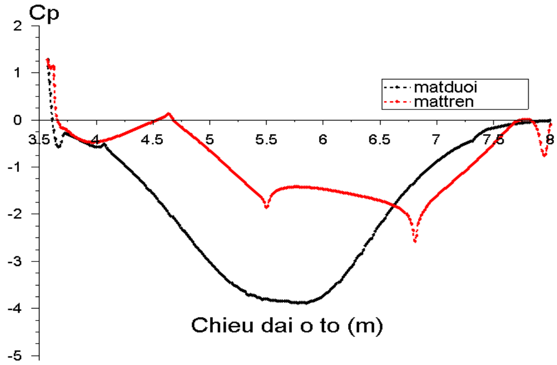

Fig 15: Pressure coefficient distribution on the car when α =22^0

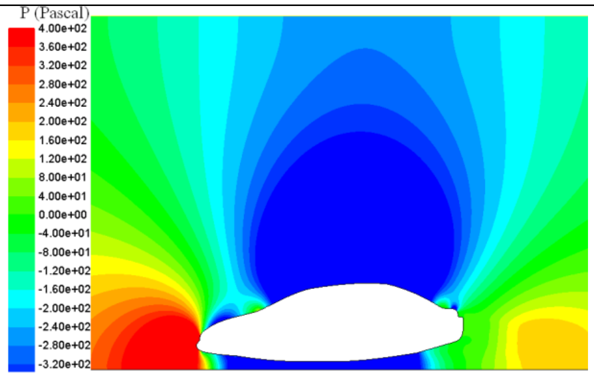

Fig 10: Pressure distribution on the calculation domain when α =25^0

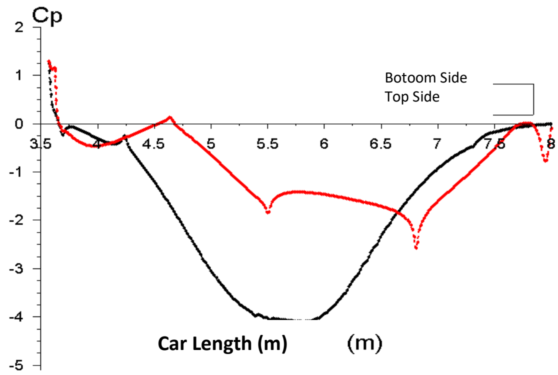

Fig 11: Pressure coefficient distribution on car when α =25^0

The results of the calculation of the drag and lift values that vary with α are shown in Table 4.

Table 5: Drag and lift values depending on the forward maneuvering angle α

α (degree)	**18**	**20**	**22**	**25**
C_d	0,345	0,304	0,29	0,258
D (N)	666,497	587,290	560,244	498,424
C_L	-5,11	-4,07	-3,97	-3,89
L (N)	987,1886	786,2735	766,9548	751,4998

Comment

In the above section, the simulation of the change in the drag coefficient C_d when changing the front maneuver angle α of the car is shown. When increasing the front maneuver angle, the pressure distribution on the underside of the car increases, so the car always tends to be lifted, causing the car's grip to decrease. The pressure above the car does not seem to change much. Therefore, in car design, the existence of an air flow below is undesirable. Under the car, there are many parts such as the engine, drive shaft, gearbox and some other parts exposed under the floor of the car. These parts block the air flow, causing turbulence as well as vortexing of the air flow below the floor of the car. Slow-moving air flows are the cause of increased lift according to Bernoulli's principle. In racing cars, people pay little attention to the maneuverability factor, to reduce aerodynamic drag, the front maneuver angle is significantly reduced. (Pham M.V., Plourde F. and Doan Kim S., 2003) [7].

3.2. Effect of rear maneuver angle β

In this section we consider the effect of aerodynamic forces acting on the car when the rear maneuver angle changes, the front maneuver angle α = 24^0.

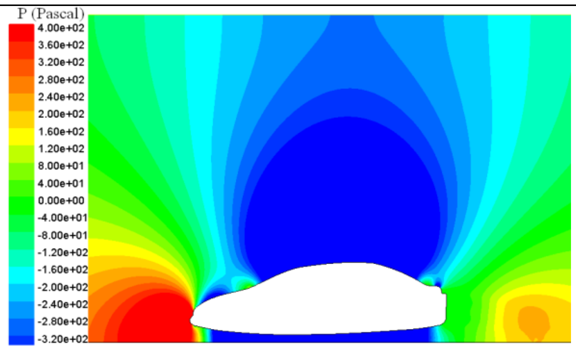

Fig 12: Pressure distribution on the calculation domain when β =16^0

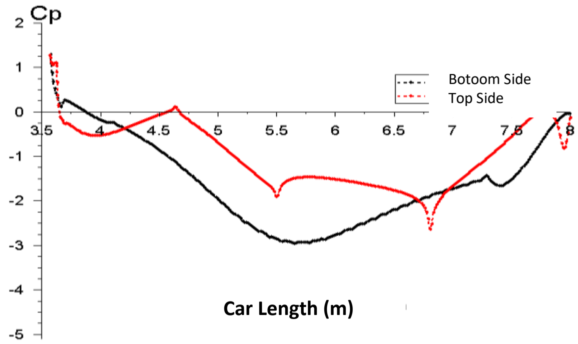

Fig 13: Pressure coefficient distribution on car when β =16^0

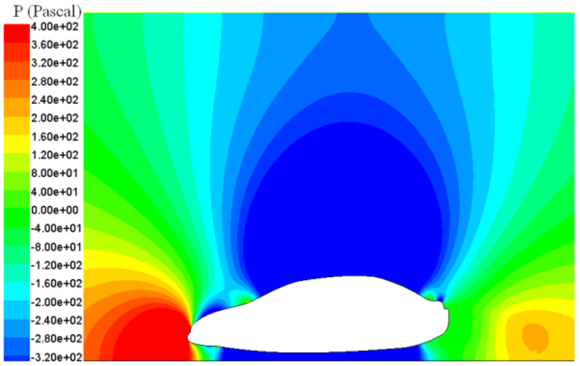

Fig 14: Pressure distribution on the calculation domain when β =18^0

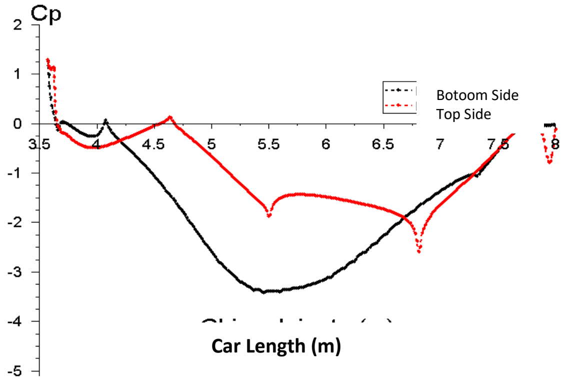

Fig 15: Pressure coefficient distribution on car when β =18^0

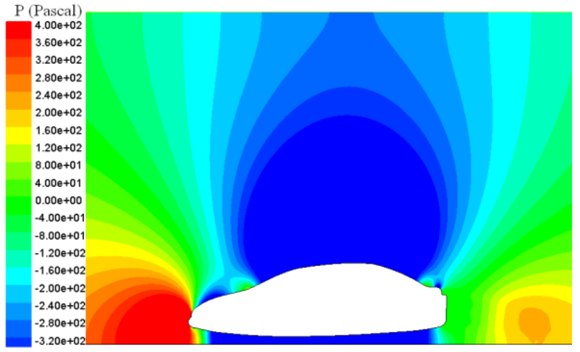

Fig 16: Pressure distribution on the calculation domain when β =20^0

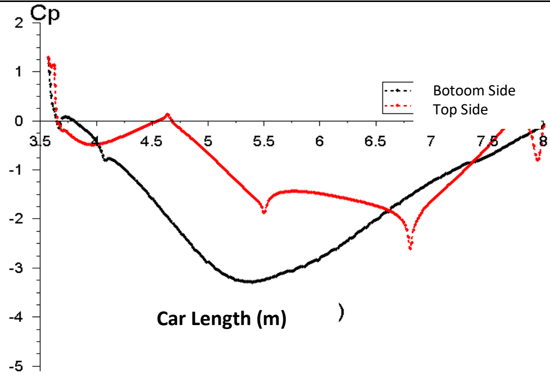

Fig17: Pressure coefficient distribution on car when β =20^0

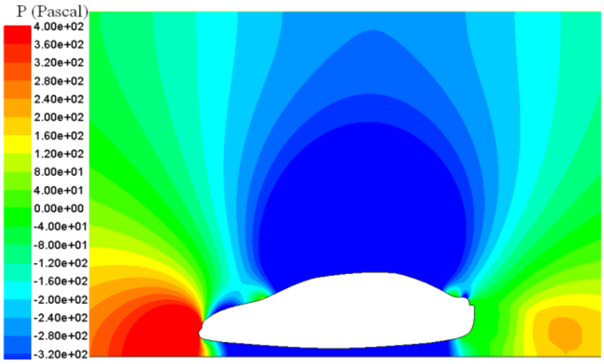

Fig 18: Pressure distribution on the calculation domain when β =22^0

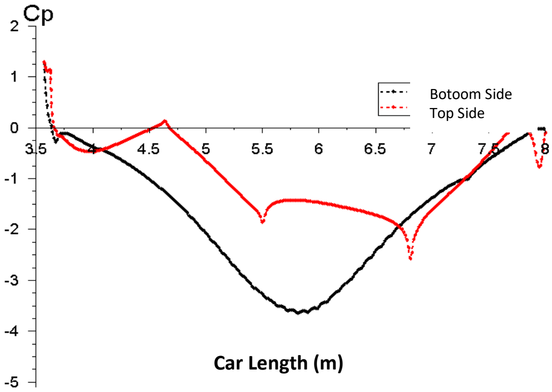

Fig 19: Pressure coefficient distribution on the car when β =22^0

The results of the calculation of the drag and lift values that vary with β are shown in Table 5

Table 6: Drag and lift values depending on the rear maneuvering angle β

β (degree)	16	18	20	22
C_d	0,265	0,263	0,262	0,262
D (N)	511,947	508,083	506,151	506,151
C_L	-3,35	-3,29	-2,67	-2,65
L (N)	647,1785	635,5872	516,3904	511,9471

4. Comment

Based on the simulation results, in the case of the rear maneuver angle increasing, the pressure on the underside of the car decreases (shown on the pressure distribution graph). This is very similar to the outside reality, when the rear maneuver angle is large, the air flow under the car floor quickly escapes to the rear, which will reduce the vortex phenomenon under the car floor, thus also reducing the lifting force acting on the car. Therefore, for cars with high mobility (large front maneuver angle), in order to reduce the air resistance acting on the car, the rear maneuver angle is also designed to be as large as the front maneuver angle. (Pham M.V., Plourde F. and Doan Kim S., 2003) [7].

The pressure distribution on the top of the car also does not change much when changing the rear maneuver angle, so the force pressing the car down does not change much, so when designing the rear maneuver angle of the car, it is necessary to pay attention to the lifting force of the car, so that the value of this force is within the allowable limit, when the car is running at high speed, the car will not overturn. (Lamballais E., Sylvestrini S.H., 2002) [10].

5. Conclusion

In this paper, the LES flow modelling method has been applied to solve the square envelope flow problem in two different Reynolds numbers. The results show the adaptability of the LES flow modelling method to the experimental data in terms of both mean and time-varying values. The calculated results are also compared with some results of other authors using the model k-ε, showing the advantage of the best response time of the LES method.

Despite its many advantages over the linear model k-ε, the LES method using the Smagorinsky model still has many issues that need to be developed to better match experimental results. For example, the value of the constant $C_s = 0.15$ is chosen in most problems, but this value can be calculated if the LES method with the dynamic constant is used. And finally, what the authors want to say here is just the initial research part of the LES method that can give the flow through a square. But it is also a foundation for studying the application of this LES method to problems with complex shapes as well as industrial flow problems.

The simulation calculation using Fluent software as a virtual laboratory achieved the following results: The rear maneuvering angle of the car is from 22^0 to 25^0, the corresponding drag coefficient C_d = 0.26, will reduce the vortex of the air flow under the car floor, reducing the lift coefficient. Research on the influence of crosswind force on the car. The simulation calculation results are a source of documents for car designers to come up with some solutions in arranging and adjusting car parts. Choosing the optimal speed for each specific car profile. Compare the simulation results using the k-ε turbulence model with other models and Fluent software with other software to be able to come up with the most optimal solution method.

References

1. Piomeli U. High Reynolds number calculations using the dynamic subgrid-scale stress model. Phys Fluids. 1993;5:1484.
2. Smagorinsky J. General circulation experiments with the primitive equations. Mon Weather Rev. 1963;91(3):99-164.
3. Lyn DA, Rodi W. The flapping shear layer formed by flow separation from the forward corner of a square cylinder. J Fluid Mech. 1994;267:353-376.
4. Lyn DA, Einav S, Rodi W. A laser-Doppler velocimetry study of ensemble-averaged characteristics of the turbulent near wake of a square cylinder. J Fluid Mech. 1995;304:285-319.
5. Durao DF, Heitor MV, Pereira JCF. Measurement of turbulent and periodic flows around a square cross-section cylinder. Exp Fluids. 1988;6:298-304.
6. Najm HN, Wyckoff PS, Knio OM. A semi-implicit numerical scheme for reacting flow. J Comput Phys. 1998;143:381-402.
7. Pham MV, Plourde F, Doan Kim S. LES simulation in a thin liquid film submitted to high thermal stress. In: ASME Summer Heat Transfer Conference; 2003 Jul 21-23; Las Vegas, NV, USA.
8. Franke R, Rodi W. Calculation of vortex shedding past a square cylinder with various turbulence models. In: Proceedings of the 8th Symposium on Turbulent Shear Flows; 1991.
9. Lamder BE, Kato M. Modelling flow-induced oscillations in turbulent flow around a square cylinder. In: Proceedings of the Forum on Unsteady Flow (FED); 1993; vol. 157. ASME.
10. Lamballais E, Sylvestrini SH. Direct numerical simulation of interactions between a mixing layer and wake around a cylinder. J Turbulence. 2002;3:28.
11. Khoa BQ. Researching, designing, and manufacturing of the pollen bee vacuum dryer model. Ho Chi Minh City University of Technology; 2010.
12. Khoa BQ. Vietnam's renewable energy industry's approach to market development: impact of smart grid systems and renewable energy sources integration. Int J Multidiscip Res Growth Eval. 2024;5(6):857-872. doi:10.54660/IJMRGE.2024.5.6.857-872.
13. Ngoc TM, Khoa BQ. Simulate energy in buildings according to LEED & LOTUS. Certification Science & Technology Publisher; 2023.
14. Ngoc TM, Khoa BQ. LEED rating system basis for green buildings. Certification Science & Technology Publisher; 2022.
15. Khoa BQ, Hay N, Duc LA, Tam PH. Optimization of the vacuum drying process for bee pollen using the R method. Int J Multidiscip Comprehensive Res. 2024;3(6):51-56. doi:10.54660/IJMCR.2024.3.6.51-56.
16. Cong NC, Vuong PM, Nghia LTM, Khoa BQ. CFD simulation of convective air flow through a square cylinder. Int J Multidiscip Comprehensive Res. 2024;3(6):57-62. doi:10.54660/IJMCR.2024.3.6.57-62.
17. Cong NC, Vuong PM, Nghia LTM, Khoa BQ. CFD simulation of air flow through a square column. Int J Soc Sci Exceptional Res. 2024;5(6):955-966. doi:10.54660/.IJMRGE.2024.5.6.955-966.
18. Khoa BQ. Simulation optimization of vacuum drying process for bee pollen using R software. Int J Soc Sci Exceptional Res. 2024;5(6):978-1013. doi:10.54660/.IJMRGE.2024.5.6.978-1013.
19. Khoa BQ. Vietnam's renewable energy industry's approach to market development: offshore renewable energy and development orientation in Vietnam. Int J Multidiscip Res Growth Eval. 2025;6(1):299-317. doi:10.54660/.IJMRGE.2025.6.1.299-317.
20. Nguyen NT, Nghia LTM, Khoa BQ. CFD application simulation & research on the influence of maneuver angle on aerodynamic forces used on cars. Int J Multidiscip Res Growth Eval. 2025;6(1):292-298. doi:10.54660/.IJMRGE.2025.6.1.292-298.